

Recent zoonotic spillover and tropism shift of a Canine Coronavirus is associated with relaxed selection and putative loss of function in NTD subdomain of spike protein.

Jordan D. Zehr¹, Sergei L. Kosakovsky Pond¹, Darren P. Martin², Kristina Ceres³, Gary R. Whittaker⁴, Laura B. Goodman⁵, and Michael J. Stanhope^{*3}.

1. Institute for Genomics and Evolutionary Medicine, Temple University, Philadelphia, PA, 19122, USA.

2. Computational Biology Division, Department of Integrative Biomedical Sciences, Institute of Infectious Diseases and Molecular Medicine, University of Cape Town, Observatory, Cape Town, South Africa.

3. Department of Population Medicine and Diagnostic Sciences, Cornell University, Ithaca, NY, 14853, USA.

4. Department of Microbiology and Immunology, Cornell University, Ithaca, NY, 14853, USA.

5. Baker Institute for Animal Health, Cornell University, Ithaca, NY, 14850, USA.

*Author to whom correspondence should be addressed: mjs297@cornell.edu

1 **ABSTRACT**

2 A recent study reported the occurrence of Canine Coronavirus (CCoV) in
3 nasopharyngeal swabs from a small number of patients hospitalized with pneumonia during a
4 2017-18 period in Sarawak, Malaysia. Because the genome sequence for one of these isolates
5 is available, we conducted comparative evolutionary analyses of the spike gene of this strain
6 (CCoV-HuPn-2018), with other available *Alphacoronavirus* 1 spike sequences. The most N-
7 terminus subdomain (0-domain) of the CCoV-HuPn-2018 spike protein has sequence similarity
8 to Transmissible Gastroenteritis Virus (TGEV) and CCoV2b strains, but not to other members of
9 the type II Alphacoronaviruses (i.e., CCoV2a and Feline CoV2-FCoV2). This 0-domain in CCoV-
10 HuPn-2018 has evidence for relaxed selection pressure, an increased rate of molecular
11 evolution, and a number of unique amino acid substitutions relative to CCoV2b and TGEV
12 sequences. A region of the 0-domain determined to be key to sialic acid binding and
13 pathogenesis in TGEV had clear differences in amino acid sequences in CCoV-HuPn-2018
14 relative to both CCoV2b (enteric) and TGEV (enteric and respiratory). The 0-domain of CCoV-
15 HuPn-2018 also had several sites inferred to be under positive diversifying selection, including
16 sites within the signal peptide. Downstream of the 0-domain, FCoV2 shared sequence similarity
17 to the CCoV2b and TGEV sequences, with analyses of this larger alignment identifying
18 positively selected sites in the putative Receptor Binding Domain (RBD) and Connector Domain
19 (CD). Recombination analyses strongly implicated a particular FCoV2 strain in the recombinant
20 history of CCoV-HuPn-2018 with molecular divergence times estimated at around 60 years ago.
21 We hypothesize that CCoV-HuPn-2018 had an enteric origin, but that it has lost that particular
22 tropism, because of mutations in the sialic acid binding region of the spike 0-domain. As
23 selection pressure on this region was reduced, the virus evolved a respiratory tropism,
24 analogous to other *Alphacoronavirus* 1, such as Porcine Respiratory Coronavirus (PRCV), that
25 have lost this region entirely. We also suggest that signals of positive selection in the signal
26 peptide as well as other changes in the 0-domain of CCoV-HuPn-2018 could represent an

27 adaptive role in this new host and that this could be in part due to the different spatial
28 distribution of the N-linked glycan repertoire for this strain.

29

30 **1. Introduction**

31 The ongoing coronavirus (CoV) disease 19 (COVID-19) is the third documented animal
32 to human CoV spillover, (SARS-CoV; SARS-CoV-2 and MERS-CoV), within the past two
33 decades, to have resulted in a major epidemic. Coronaviruses (CoVs) that infect mammals (with
34 the exception of pigs) belong principally to two genetic and serologic groups:
35 the *Alphacoronavirus* (α) and *Betacoronavirus* (β) genera. *Alphacoronavirus* 1 is a species
36 within the *Alpha* genus which comprises viruses that infect dogs, cats and pigs, and is further
37 subdivided into type I and II based on serological parameters and genetic differences in the
38 spike gene, although further genetic and biological differences are also apparent (see for e.g.,
39 CCoV1; Decaro et al. 2015). Vlasova et al. (2021) recently reported on an *Alphacoronavirus* 1
40 CoV resembling Canine CoV (CCoV), isolated from nasopharyngeal swabs of a small number of
41 patients (8/301; seven of these eight were children), in Sarawak Malaysia, hospitalized with
42 pneumonia during a 2017-18 period. The genome sequence of one of these isolates was
43 obtained, while the other seven were diagnosed based on PCR tests. Genomically, the virus
44 resembles a CCoV type II, but also shares high nucleotide sequence similarity with other type II
45 *Alphacoronavirus* 1 viruses: feline CoV (FCOV2), and the porcine Transmissible Gastroenteritis
46 Virus (TGEV).

47 Zoonotic transmissions of CoVs represent an important threat to human health, with
48 many unknown possible reservoir hosts. The Vlasova et al. report is the first example of a
49 Canine CoV isolated from a human patient with pneumonia, although the virus has not been
50 confirmed as the causative pathogen and inter-individual transmission has not been
51 established. However, the obvious importance of a jump from a companion animal such as a
52 dog or a cat, or from a farm animal such as a pig, to a human host, raises concerns and

53 questions about possible adaptative tropism of veterinary coronaviruses to humans. A key
54 component of CoV host tropism is the binding of the spike protein with host cellular receptors.
55 The spike protein is responsible for host receptor binding and fusion of the virus and host cell
56 membranes (Li, 2016). It is comprised of the N-terminal S1 region, containing the receptor
57 binding domain (RBD), and the C-terminal S2 region, responsible for membrane fusion. The
58 CCoV receptor in dogs, and for the rest of the type II members of the *Alphacoronavirus 1*
59 species, is amino peptidase N (APN) (reviewed in Millet et al. 2021). The human common-cold
60 coronavirus, HCoV-229E, another *Alphacoronavirus*, (not *Alphacoronavirus 1*) also uses APN.
61 Structural studies involving porcine respiratory coronavirus (PRCV; closely related to TGEV)
62 indicate that it binds to a site on porcine APN that differs from the site at which HCoV-229E
63 binds to hAPN (Reguera et al. 2012; Wong et al. 2017), implying that there are multiple ways for
64 this interaction to take place. Importantly, feline APN can serve as a functional receptor of type
65 II CCoV, TGEV and human coronavirus HCoV-229E (Tresnan, Levis and Holmes 1996). While
66 definitive experimental data are still lacking, the possibility of co-infections in cats implies that
67 individual cells can become infected with these different CoVs, which could, in turn, generate
68 novel recombinant strains. Spike gene recombination has played an important role in the
69 evolution of the *Alphacoronavirus 1* type II CoVs, involving recombination between dog, cat and
70 pig viruses, including the complete replacement of the most N-terminus subdomain of CCoV2
71 with that of TGEV - an important event in the formation of CCoV2b (Wesley 1999). In keeping
72 with this aspect of the *Alphacoronavirus 1* group's history, Vlasova et al., provide evidence that
73 CCoV-CCoV-HuPn-2018 carries a recombinant CCoV/FCoV spike gene.

74 In addition to APN, alternative attachment factors and/or co-receptors are also known for
75 some *Alphacoronavirus 1* CoVs, including C-type lectins dendritic cell-specific intercellular
76 adhesion molecule-3-grabbing non-integrin (DC-SIGN), heparan sulfate (HS), and sialic acid
77 (reviewed in Millet et al. 2021). Thus, there are numerous possible avenues for developing new
78 receptor interactions, an important step in cross-species transmission. Key mutations in the

79 spike gene of a CCoV such as CCoV-HuPn-2018, acquired either through recombination or
80 diversifying selection, could facilitate adaptation to a new host's receptor(s). Here, we provide a
81 further perspective on the recombination history involving the spike gene of CCoV-HuPn-2018,
82 with other members of the *Alphacoronavirus* 1 type II species, and characterize selection
83 pressures across the spike gene, focusing on where such events are in relation to spike
84 functional domains.

85

86 **2. Methods**

87 **2.1 Sequences and alignments**

88 We collected complete spike gene sequences from *Alphacoronavirus* 1 type II CoVs
89 available in GenBank (accession numbers appear in Supplementary Table S1). Partial spike
90 sequences of *Alphacoronavirus* 1 were excluded from our analysis, as were strains determined
91 from associated publications, to have been be serially passaged (including experimental
92 inoculations of any kind). CCoV type II viruses are currently split into two groups: CCov2a and
93 CCoV2b. Our choice of CCoV2b as our representative CoV from the dog host is based on the
94 fact the most N-terminus subdomain of the spike protein of CCoV2b and TGEV share sequence
95 similarity to CCoV-HuPn-2018, whereas this is not the case for either CCoV2a or FCoV2. Spike
96 domain site positional mapping is based on serotype I feline infectious peritonitis virus (FIPV;
97 Yang et al. 2020) which is the only *Alphacoronavirus* 1 with a currently available spike protein
98 crystal structure. Although a similar domain map is not available for type II *Alphacoronavirus* 1s,
99 there is sufficient amino acid sequence similarity between type II *Alphacoronavirus* 1s and FIPV
100 to either closely approximate site positions (e.g., for N terminal subdomains) or to more
101 precisely pinpoint site positions (e.g., RBD). Type I and type II *Alphacoronavirus* 1 viruses were
102 not included together in sequence alignments used for selection analyses, because of the
103 divergence between these two types.

104 We prepared two sets of alignments for comparative sequence analyses. The first of
105 these (set I) included TGEV, CCoV-HuPn-2018, and the CCoV2b strains. This set of sequences
106 was assembled for the analysis of the N-terminus subdomain and we only consider results
107 involving the first 288 aligned amino acid positions (up to and including position 266 of CCoV-
108 HuPn-2018) referred to as the 0-domain in the FIPV structural paper (Yang et al. 2020), and
109 here. The second set (set II) included all strains, and positions downstream of 289, which
110 represents the beginning of the region where FCoV2 and the other sequences share a high
111 degree of sequence similarity. In-frame nucleotide sequences were translated to amino-acids,
112 aligned with MAFFT (Kato and Standley 2013), and then mapped back to the nucleotide
113 sequences to produce a codon-aware alignment. The resulting alignments were largely gapless,
114 with the exception of two short regions of indels in alignment set I (specifically, the 0-domain).
115 We excluded these regions from positive selection analyses, since uncertain alignment is known
116 to degrade method performance.

117

118 **2.2 Positive selection and recombination**

119 Both alignment sets were screened for recombination with breakpoints identified using
120 GARD (Kosakovsky Pond et al. 2006); set II was also evaluated with RDP5 (Martin et al. 2020)
121 for an additional level of granularity with regard to determining the polarity of sequence
122 exchanges. Each of the resulting GARD fragments served as input to the selection analyses,
123 concomitant with their respective phylogeny, which was inferred using RaxML (Stamatakis
124 2014) under the GTR+ Γ nucleotide substitution model.

125 We performed site-, branch-, and alignment-level selection tests based on the dN/dS
126 (nonsynonymous / synonymous) ratio estimation as implemented in the HyPhy software
127 package v.2.5.31 (Kosakovsky Pond et al. 2020). We used the MEME method (Murrell et al.
128 2012) to look for episodic diversifying selection pressure at individual sites across the entire tree
129 (both sets I and II). We tested the CCoV-HuPn-2018 terminal branch for evidence of selection,

130 both overall (some subset of sites along this branch), using the aBSREL (Smith et al. 2015), and
131 BUSTED (Murrell et al. 2015) methods, and at individual sites using the FEL (Kosakovsky Pond
132 et al. 2005) and MEME (Murrell et al. 2012) methods. We modified the FEL and MEME tests to
133 use parametric bootstrap for estimating the null distribution of the likelihood ratio test instead of
134 the asymptotic distribution used in the published tests. This was done to improve the statistical
135 performance of the tests, when the test set comprises a single branch, with the tradeoff of a
136 significant increase in computational cost. We used 100 parametric bootstrap replicates to
137 generate the distribution of the test statistic under the null hypothesis (neutral evolution or
138 negative selection).

139

140 **2.3 Estimating divergence times**

141 **2.3.1 Temporal signal**

142 The temporal signal in each GARD partition was assessed using root-to-tip regression in
143 TempEst v1.5.3 (Rambaut et al. 2016) and tip-dating-randomization tests (TDR) (Duchêne et al.
144 2015). First, ModelFinder (Kalyaanamoorthy et al. 2017) was used in IQTREE-2 (Minh et al.
145 2020) to identify the best fitting substitution model for each alignment using Bayesian
146 Information Criterion (BIC). Each tree with the best-fitting substitution model was then used as
147 input for root-to-tip regression analysis, where correlation coefficients were calculated using the
148 heuristic residual mean squared function. If a strong temporal signal exists (a linear relationship
149 between genetic distance and sampling time), the correlation coefficient will be positive. For
150 GARD partitions with correlation coefficient greater than 0.1, temporal signal was confirmed
151 using TDR. The R package TipDatingBeast (Rieux et al. 2017) was used to generate ten
152 random permutations of sample dates for each GARD alignment. BEAST2 (Bouckaert et al.
153 2014) was then used to estimate the evolutionary rate for both alignments with the true sample
154 dates and alignments for each randomized replicate. If the mean clock rate estimate of the

155 alignment with real sample dates fell outside the 95% highest posterior density (HPD) for the
156 randomized date set, temporal signal was deemed sufficient for subsequent analyses.

157

158 **2.3.2 Model selection**

159 For each alignment that had sufficient evidence of a temporal signal, the fit of
160 combinations of two molecular clock models (strict and uncorrelated relaxed exponential
161 Drummond et al. 2006)) and two demographic models (constant coalescent and Bayesian
162 skyline plot (Drummond et al. 2005)) were assessed using marginal likelihood estimation. For
163 each model tested, marginal likelihood was calculated using PathSampling (Lartillot & Philippe
164 2006) within the Model-Selection package in BEAST 2 with 12 steps, 1,000,000 MCMC steps
165 with 25% burn-in, and an alpha of 0.3. The average marginal likelihood estimates from two path
166 sampling runs were compared to other model combinations using Bayes Factors (Kass &
167 Raftery 1995).

168

169 **2.3.3 Discrete trait analysis**

170 The ancestral state of host species (cat, dog, pig, human) was inferred using discrete
171 ancestral trait mapping in BEAST2 (Bouckaert et al. 2014) for each GARD alignment. Bayesian
172 phylogenies were created using 100 million MCMC steps in BEAST2, sampling every 10,000
173 steps. Trees were summarized using the BEAST2 package TreeAnnotator v2.6.0, discarding
174 20% of trees as burn-in. Convergence of the MCMC chains was assessed using Tracer
175 v1.7.1(Rambaut et al. 2018) and the effective sample size for each estimated parameter was
176 confirmed to be greater than 200. Phylogenetic trees were annotated using FigTree v1.4.4
177 (available from <http://tree.bio.ed.ac.uk/software/figtree/>).

178

179

180

181 3. Results

182 3.1 GARD partition topologies and positive selection

183 GARD identified two recombinant partitions in the N-terminal subdomains comprising
184 alignment set I, and eight partitions for the remaining regions of the spike gene for alignment set
185 II. The first alignment set I GARD partition included nearly all of the 0-domain (amino acid
186 alignment positions 1-230; position 220 of CCoV-HuPn-2018; FIPV coordinate 235); the second
187 GARD partition from alignment set I overlaps with the downstream onset of sequence similarity
188 between FCoV2, CCoV2b, TGEV and CCoV-HuPn-2018 (which begins at alignment position
189 289; position 267 of CCoV-HuPn-2018; FIPV coordinate 287; Fig. 1). The phylogeny of

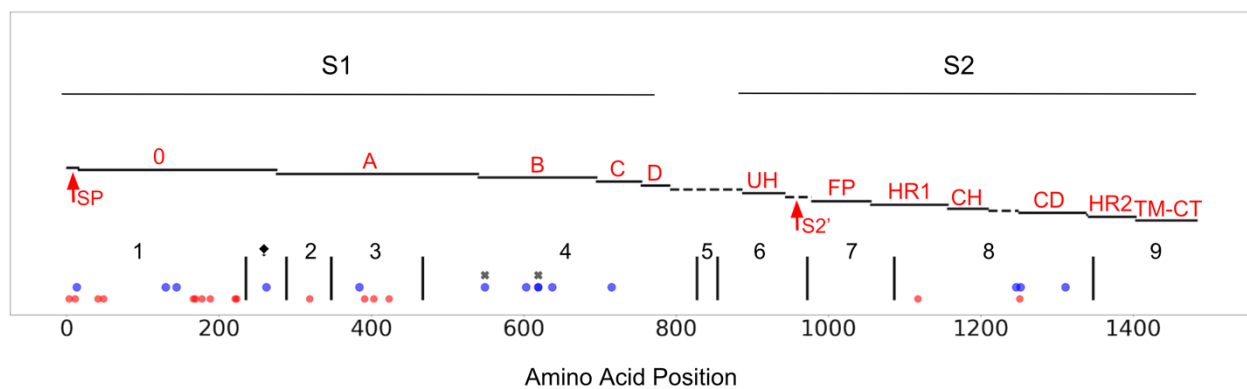


Fig. 1. CCoV-HuPn-2018 spike protein, mapped to a published FIPV-UU4 spike gene map (Yang et al. 2020). S1, S2, of spike are highlighted and the protein is further subdivided into functional subunits and subdomains. Blue dots represent sites under positive selection in CCoV-HuPn-2018 as identified by MEME and FEL in the single branch tests; red dots represent sites that are unique in CCoV-HuPn-2018, but are not under positive selection; black "x"s indicate sites under positive selection in the MEME test of the complete alignment that had moderate EBF values for CCoV-HuPn-2018. Red text labels accompany each subdomain/functional unit and are based on the original FIPV spike structure (Yang et al. 2020): SP, signal peptide; 0 domain; A domain; B, includes RBD-Receptor-Binding Domain; C; D; UH, upstream helix; S2', S2' cleavage (predicted furin site, using ProP1.0 (Duckert et al. 2004)); FP, fusion peptide; HR1, heptad repeat region 1; CH, central helix; CD, connector domain; HR2, heptad repeat region 2; TM, transmembrane domain; CT, cytoplasmic tail. The dashed line between D and UH refers to a region of peptide with no sequence similarity between FIPV and CCoV-HuPn-2018; this region includes the S1/S2 furin cleavage site in FIPV, which is absent in CCoV-HuPn-2018. The vertical black lines represent the breakpoints of the GARD identified non-recombinant fragments, and are labeled numerically. The ◆ symbol represents a 3' GARD fragment of alignment set I that was analyzed for positive selection; this GARD fragment was determined from an alignment of just CCoV2b and TGEV sequences (set I). The 5' end of GARD fragment 2 represents the onset of FCoV2 sequence similarity (set II).

190

191 GARD partition 1 (Supplementary Fig. S1) includes CCoV-HuPn-2018 as a separate branch
192 intermediately placed between the CCoV2b and TGEV sequences. Phylogenies of the eight
193 GARD partitions for alignment set II (Supplementary Fig. S1) had CCoV-HuPn-2018 in various
194 topological positions including: closely related to one or more CCoV2b sequences (GARD
195 partitions 2, 4, 9), intermediate between dog/cat and pig viruses (GARD partition 3), and as a
196 sister group to FCoV2 sequences (GARD partitions 3, 5, 6, 7, 8). MEME analysis of the 0-
197 domain (alignment set I) did not identify any positively selected sites, whereas the same
198 analysis of alignment set II identified a total of 9 sites at $P \leq 0.05$. Two of these sites overlapped
199 with the single branch tests involving CCoV-HuPn-2018 and had moderate Empirical Bayes
200 Factor values (Fig. 1; EBFs: 128, 48 – sites 549 and 619 respectively); these two sites were in
201 the RBD region of the protein (Fig. 1). The remainder of the MEME sites were identified with
202 supportive EBF values on an assortment of CCoV2b and FCoV2 branches. MEME analysis
203 restricted to the CCoV-HuPn-2018 branch, identified a total of 11 positively selected sites, four
204 in the 0-domain (one in the signal peptide, which was identified with SIGNALP-5.0 (Almagro
205 Armenteros et al. 2019)), three in RBD, one in the C-domain, and three in or adjacent to the
206 Connector Domain (CD) (Fig. 1). FEL analysis of the CCoV-HuPn-2018 branch identified four
207 sites, three of which overlapped with the MEME single branch test, and one unique site in RBD
208 (Fig. 1; positive selection statistics summarized in Supplementary Table S2). aBSREL and
209 BUSTED analyses restricted to the CCoV-HuPn-2018 branch did not identify significant
210 evidence of segment-wide selection pressure, however both aBSREL and BUSTED are known
211 to have lower power when the test branch set is small (Murrell et al. 2015; Smith et al. 2015).

212

213 **3.2 Recombination**

214 RDP5 was used to analyze recombination events in alignment set II which contained
215 FCoV2, CCoV2b, TGEV and CCoV-HuPn-2018 sequences. Because it is not possible to have
216 all natural occurring sequence variants represented in any alignment, it should be noted that

217 when we refer to a sequence as a donor in the following descriptions, it applies to, and is limited
218 by, the sequences in this alignment, and that other closely related genetic variants could be the
219 precise donor. A total of 19 recombination events were well supported (Table S3) by a subset of
220 three or more of the recombination detection methods implemented in RDP5 including BURT,
221 RDP, MaxChi (Smith 1992) and GENECONV (Padidam et al 1999;). Of the 19 supported
222 events, five implicate the CCoV-HuPn-2018 sequence as either a possible recombinant (two
223 events) or as a genetic donor sequence (three events; Supplementary Fig. S2). In the two
224 recombination events where CCoV-HuPn-2018 is the proposed recombinant sequence the
225 putative genetic donors are FCoV2 (strain M91-267, accession AB781788.1) and TGEV (strain
226 TGEV/USA/Tennessee144/2008, accession KX900401.1), and CCoV2b (strain 341/05,
227 accession EU856361.1) and TGEV (strain JS2012, accession KT696544.1), events 13 and 19
228 respectively. There are three well supported recombination events where CCoV-HuPn-2018 is
229 suggested as the genetic donor, and each event involves a second donor in a strain other than
230 CCoV-HuPn-2018 (i.e., one event with each of FCoV2, CCoV2b, and TGEV respectively). The
231 three inferred recombination events are as follows: CCoV-HuPn-2018 recombines with a FCoV2
232 (strain Tokyo/cat/130627, accession AB907624.1) sequence to yield a FCoV2 recombinant
233 (strain WSU 79-1683, accession JN634064.1), CCoV-HuPn-2018 recombines with CCoV2b
234 (strain 341/05, accession EU856361.1) to yield a CCoV2b recombinant (strain 174/06,
235 accession EU856362.1), and lastly CCoV-HuPn-2018 recombines with TGEV (strain JS2012,
236 accession KT696544.1) to yield an FCoV2 recombinant (strain WSU 79-1683, JN634064.1),
237 events 5, 6, and 10 respectively. Of the 19 recombination events there are five where the
238 inferred parental sequences and recombinants all belong to different virus types (i.e., TGEV and
239 FCoV2 recombine to yield a CCoV2b) and of these five, one event (event 10) implicates CCoV-
240 HuPN-2018 as a proposed genetic donor, and one (event 13) implicates it as a proposed
241 recombinant.

242 **3.3 Temporal analysis**

243 GARD partition 7 had substantive temporal signal in the root-tip-regression and TDR
244 analyses. Four other partitions had correlation coefficients greater than 0.1 on the root-tip-
245 regression tests (Table S4) but failed the TDR, so only GARD partition 7 was used in the
246 temporal analysis (Supplementary Fig. S3). Ancestral host state and lineage divergence times
247 for the GARD 7 partition are shown in Supplementary Fig. S4. CCoV-HuPn-2018 likely diverged
248 from a lineage most recently circulating in cats between 1846 and 1976 (95% HPD – Highest
249 Posterior Density Interval), with a median estimate of 1957. Additional possible host shifts are
250 noted throughout the evolutionary history of the GARD 7 partition including another cat to dog
251 host jump around or after 1981, 95% HPD = [1882, 2005].

252

253 **4. Discussion**

254 We found moderate statistical evidence of positive selection acting upon sites in various
255 regions of the spike gene, primarily at specific sites of the CCoV-HuPn-2018 branch. The 0-
256 domain of CCoV-HuPn-2018 (GARD partition 1; Fig. 1) had seven unique amino acid residues
257 relative to the sequences in the set II alignment, two of which were inferred to be evolving under
258 positive selection (one in the signal peptide). This portion of the CCoV-HuPn-2018 NTD
259 comprises 288 residues with homology only to available TGEV and CCoV2b isolates. Earlier
260 studies have reported on this similarity, implicating recombination between CCoV2 and TGEV
261 (Wesley 1999; Decaro et al. 2009) in the origins of CCoV2b (Wesley 1999). These recombinant
262 CCoV2b are circulating among the domestic dog population (Decaro et al. 2009). The 0-domain
263 region (Fig. 1) is subject to relaxed selection (analysis conducted with RELAX - Wertheim et al.
264 2015) compared to the other CCoV sequences (GARD partition 1; RELAX results: $K=0.07$;
265 $p=0.005$). It has an increased rate of molecular evolution relative to the other CCoV and TGEV

266 sequences (significant Tajima's relative rate test, implemented in MEGA X – Kumar et al. 2018;
267 all three codon positions, as well synonymous alone, and for most nonsynonymous pairwise
268 comparisons). This selective relaxation suggests that at least some of the history of CCoV-
269 HuPn-2018 involves the loss of function or loosening of functional constraints of this domain,
270 and may also suggest that this region may have different functional roles in humans and dogs.

271 The role of spike NTD domains in CoV infections is increasingly being recognized. The
272 NTD may act as a co-receptor for SARS-CoV-2, interacting with tyrosine-protein kinase receptor
273 UFO (AXL; Wang et al. 2021) and possibly sialic acids (reviewed in Sun 2021). Sialic acid
274 binding in the NTD has been confirmed for TGEV and PEDV (Schultze et al. 1996; Liu et al.
275 2015). Point mutations or a short deletion near the N-terminus in TGEV eliminate sialic acid
276 binding, and are associated with lower viral pathogenicity (Krempl et al. 1997). The complete
277 absence of the O-domain in porcine respiratory coronavirus (PRCV; closely related to TGEV),
278 which includes the region involved in the Krempl et al (1997) experiments, eliminated sialic acid
279 binding (Rasschaert et al. 1990). This O-domain deletion and the resulting loss in sialic acid
280 binding led to a switch in tropism and pathogenicity for PRCV to predominantly respiratory tract-
281 tropic (Krempl et al. 1997). TGEV on the other hand can infect both the respiratory and enteric
282 tracts (Sanchez et al. 2019). A human respiratory *Alphacoronavirus* - HCoV-229E -
283 hypothesized to have originated in bats, is also missing this region (Corman et al. 2015). Krempl
284 et al. identified, and experimentally confirmed, a ten-residue region of the O-domain that is
285 essential for TGEV pathogenicity. This same region in our TGEV/CCoV2b/CCoV-HuPn-2018
286 alignment has three amino acid changes and one amino acid deletion in CCoV-HuPn-2018
287 relative to TGEV (and no changes in TGEV). Regions upstream and downstream of these ten
288 amino acids are strongly conserved. This general region of the sequence, between 143-168 of
289 our alignment (Supplementary Fig. S5; 143-153 of CCoV-HuPn-2018 sequence), is the most
290 variable section of the O-domain across these viruses, with two gaps to accommodate two six

291 amino-acid insertions in the CCoV2b sequences. Although these CCoV2b insertions are of the
292 same length, they differ in amino acid composition.

293 In summary: (a) CCoV-HuPn-2018, shows evidence of relaxed selection in the 0-domain
294 portion of NTD; (b) there are numerous amino acid changes for CCoV-HuPn-2018 in this region
295 that were not associated with signals of positive selection (Fig. 1); (c) the 0-domain of CCoV-
296 HuPn-2018 has an increased rate of molecular evolution; (d) unique amino acid changes, and
297 an amino acid deletion, in CCoV-HuPn-2018 are evident in a ten residue area of the 0-domain
298 experimentally determined to be key to sialic acid binding in TGEV and to affect TGEV
299 pathogenicity (e) this same specific sialic acid binding region of CCoV-HuPn-2018 shares no
300 sequence similarity to CCoV2b, as does much of the surrounding sequence, including two 6
301 amino acid insertions unique to CCoV2b – a solely enteric pathogen (f) Alpha-respiratory
302 viruses such as PRCV and HCoV-229E have lost the 0-domain; (g) CCoV-HuPn-2018 was
303 associated with a respiratory infection in the Malaysian patients. This leads us to hypothesize
304 that CCoV-HuPn-2018 had an enteric origin, has lost that particular tropism, due in part to
305 mutations in the sialic acid binding region of the 0-domain, resulting in reduced selection
306 pressure for this subdomain. Analogous to other *Alphacoronavirus 1*, such as PRCV, that have
307 lost this region entirely, it has evolved a respiratory tropism. Furthermore, we suggest the
308 possibility that the CCoV-HuPn-2018 lineage might eventually lose this region entirely, just like
309 PRCV, but that we are witnessing early stages of this process. A similar deletion of 197 amino
310 acids has been reported in the 0-domain of some strains of PEDV, an *Alphacoronavirus 2* (Oka
311 et al. 2014); in this case, without evidence of tropism shift, but with experimental evidence that
312 this deletion attenuates the virus, likely due to its loss of sialic acid binding (Hou et al. 2017).
313 Vlasova et al. in their analysis of the complete CCoV-HuPn-2018 genome, found that there is a
314 deletion in the middle of the N-protein and a truncated ORF7b compared to other CCoVs and
315 suggested this could have implications in the apparent host shift.

316 A corollary hypothesis to our ideas on the history of the CCoV-HuPn-2018 0-domain, not
317 mutually exclusive to the one we suggest above, is that the increased genetic variation for this
318 subdomain has somehow pre-adapted the virus to this host shift (see discussion by De Fine
319 Licht 2018), and that the weak signal of positive selection that we observe indicates recent
320 limited host specific adaptation, perhaps reflecting a trajectory of a novel niche expansion.
321 Under such a hypothesis the genetic differences apparent in CCoV-HuPn-2018 expose the virus
322 to new regimes of natural selection, and is analogous to discussions on the role of cryptic
323 genetic variation in facilitating adaptation to new conditions (Paaby and Rockman 2014).
324 Alternatively, the limited positive selection that we do see in this region for CCoV-HuPn-2018
325 could reflect a remnant of earlier selection in a previous host.

326 We identified four positively selected sites within the putative RBD of CCoV-HuPn-2018.
327 Based on the FIPV spike structure and the accompanying CoV alignment, only one of these four
328 positively selected sites (at position 619) is in a putative RBD extended loop: specifically, at the
329 end of extended loop 2 (cf. Fig. 4 of Yang et al. 2020). RBD extended loops form the interaction
330 points with the APN receptor in other Alphacoronaviruses (Wong et al. 2017; Yang et al. 2020;
331 Wu et al. 2009) and the specifics of the interaction between these loops and APN, even
332 between closely related viruses, can be very different (Wong et al. 2017).

333 Another region of note with evidence for positive selection in CCoV-HuPn-2018 was the
334 signal peptide. CoV signal peptides play a role in threading the polypeptide chain through the
335 host endoplasmic reticulum (ER) membrane during protein synthesis. The signal peptide is
336 recognized by the translocon and is pulled through into the ER lumen, with the rest of the
337 polypeptide following. Within the lumen, spike folds and becomes glycosylated. N-linked
338 glycosylation is a common form of viral protein modification, in which a glycan is attached to the
339 amide nitrogen of asparagine at the conserved sequence motif Asn-X-Ser/Thr. Many viruses
340 make use of this host cell process to modify surface proteins, including the spike of CoVs, and
341 this can impact antigenicity and host cell invasion. CoVs have numerous N-linked glycosylation

342 sites in the spike protein, including those structurally verified for the type I *Alphacoronavirus* 1
343 CoV FIPV (Yang et al. 2020). Recent work on HIV, which like CoV is an enveloped virus, found
344 that the signal peptide can influence the glycan profile and antigenicity of the HIV surface
345 protein gp120 (Yolitz et al. 2018), prompting these authors to suggest that despite the fact the
346 signal peptide is not part of the mature protein, it is likely to be subject to immune pressure.
347 Both the MEME and FEL methods detected positive selection at a codon in the signal peptide of
348 CCoV-HuPn-2018. There are also two additional amino acid changes in the signal peptide of
349 CCoV-HuPn-2018 that differentiate it from other CCoV2b and TGEV sequences. The inferred N-
350 linked glycosylation sites on the CCoV-HuPn-2018 and CCoV2b spike sequences (predicted
351 using NetNglyc;<http://www.cbs.dtu.dk/services/NetNGlyc/>) while mostly overlapping, have some
352 noteworthy differences: there were 26-29 (mode = 28) N-linked glycosylated sites in the
353 CCoV2b sequences, and there were 29 sites in CCoV-HuPn-2018; of these totals, 3-5 of the
354 CCoV2b sites were in the 0-domain, whereas CCoV-HuPn-2018 had seven in the 0-domain. As
355 a control we also performed the N-linked glycosylation site inference on the FIPV UU4
356 sequence using NetNglyc and identified almost all of the experimentally verified sites (Yang et
357 al. 2020) for this sequence. Thus, CCoV-HuPn-2018 appears to have a slightly different
358 repertoire of N-linked sites compared to CCoV2b, and with several of these differences
359 occurring in the 0-domain. None of these N-linked glycosylation sites were positively selected in
360 CCoV-HuPn-2018. Positive selection of sites within signal peptides has been reported for other
361 viruses, such as cytomegalovirus, where it was demonstrated that the selected variants affect
362 the timing of signal peptide removal and viral glycoprotein intracellular trafficking (Mozzi et al.
363 2020). We propose that positive selection in the signal peptide of CCoV-HuPn-2018 could
364 reflect an adaptive role in this new host and that the unique amino acid changes in the signal
365 peptide of CCoV-HuPn-2018 compared to CCoV2b and TGEV, could be playing a role with
366 regards to the N-linked glycan repertoire of this strain.

367 Given the sample of analyzed sequences there are two recombination events identified
368 by RDP5 where CCoV-HuPn-2018 is the proposed recombinant and three events where CCoV-
369 HuPn-2018, is the proposed major genetic donor of recombinantly transferred sequences
370 (Supplementary Fig. S2). Two of the recombination events identified by RDP5, at the 5' end of
371 the A-domain (events 5 and 13 in Fig. S2), have similar predicted breakpoint locations which
372 overlap almost exactly with GARD partition 2. For one of these events (event 5), CCoV-HuPn-
373 2018 is identified as a possible sequence donor and FCoV2 as a recombinant, and in the other
374 (event 13), CCoV-HuPn-2018 is the proposed recombinant with FCoV2 as the proposed donor
375 sequence. The detection of both events involved the same FCoV2 sequence (strain WSU 79-
376 1683; accession number JN634064), isolated at Washington State University in 1979
377 (McKeirnan et al. 1981). A 2009 survey of cats in two Malaysian catteries, using PCR primers
378 designed from strain WSU-79-1683 and FIPV79-1146, found a high prevalence of FCoV test
379 positives (Sharif et al. 2009). While these apparently convergent recombination events could
380 indicate a recombination hotspot, it is also plausible that either (1) there was a single
381 recombination event in FCoV2 that was misidentified as a recombination event in CCoV-HuPn-
382 2018, or (2) there were two unique recombination events, as inferred by RDP5, one in FCoV2
383 and the other in CCoV-HuPn-2018.

384 The FCoV2 JN634064 sequence is also a very close sister group to CCoV-HuPn-2018
385 for GARD partitions 2, 6, 7, and 8 (Supplementary Fig. S1), with 6-8 spanning most of the S2
386 domain. The BEAST analysis timed the split of WSU 79-1683 and CCoV-HuPn-2018 in partition
387 7 at 1957. The high prevalence of FCoV2 in Malaysian cats, suggested by the Sharif et al.
388 study, concomitant with their primer construction strategy, suggests the possibility that a WSU
389 79-1683-like virus could be the prevalent FCoV2 strain in Malaysia. There are also the
390 experimental results of Tresnan et al. (1996) which demonstrate that feline APN can serve as a
391 functional receptor of type II CCoV, TGEV and HCoV-229E, suggesting that cats may act as a
392 mixing vessel for generating recombinant *Alphacoronavirus* 1 CoVs. The origins of WSU 79-

393 1683 may also include two recombination events in the Orf1ab region with FCoV1 and CCoV as
394 sequence donors (Herrewegh et al. 1998). These observations lead us to conclude that WSU
395 79-1683, or its close relative, has had a prominent role in the evolution of CCoV-HuPn-2018 and
396 that these viruses have repeatedly coinfecting hosts, resulting in recombinant progeny.

397 We propose that at some time in the history of CCoV-HuPn-2018, its spike protein 0-
398 domain may have lost its functional significance. Importantly, other viruses in this group such as
399 PRCV, exhibit a similar evolutionary trajectory where an eventual complete loss of this region of
400 the protein is associated with a shift from enteric to respiratory tropism. Both the molecular
401 details underlying how the loss of this domain contributes to tropic shift of this sort, and the
402 reason(s) that zoonotic host shifts in CoVs are frequently coincidental with respiratory infection,
403 remain important unsolved mysteries. Timing of the origins of CCoV-HuPn-2018 to
404 approximately 1957 suggest that this virus may have been circulating undetected in humans,
405 dogs, cats, or intermediate unidentified hosts for decades. This, in turn, leads us to whole-
406 heartedly concur with the suggestions of Vlasova et al. that a systematic survey should be
407 conducted for the prevalence of CCoV-HuPn-2018 in the host species that comprise the
408 complex history of this virus.

Conflicts of interest: None declared.

Acknowledgements

This study received funding (FOA PAR-18-604) from the U.S. Food and Drug Administration's
Veterinary Laboratory Investigation and Response Network (FDA Vet-LIRN) under grant
1U18FD006993-01, awarded to LBG and MJS. SLKP and JDZ were supported in part by grants
R01 AI134384 (NIH/NIAID) and U01 GM110749 (NIH/NIGMS). We gratefully acknowledge Jean
Millet for helpful advice on *Alphacoronavirus* biology and spike structural domains.

References

- Almagro Armenteros JJ, Tsirigos KD, Sønderby CK, et al. SignalP 5.0 improves signal peptide predictions using deep neural networks. *Nat Biotechnol.* 2019;37(4):420-423. doi:10.1038/s41587-019-0036-z
- Bouckaert R, Heled J, Kühnert D, et al. BEAST 2: a software platform for Bayesian evolutionary analysis. *PLoS Comput Biol.* 2014;10(4):e1003537. doi:10.1371/journal.pcbi.1003537
- Corman VM, Baldwin HJ, Tateno AF, et al. Evidence for an Ancestral Association of Human Coronavirus 229E with Bats. *J Virol.* 2015;89(23):11858-11870. doi:10.1128/JVI.01755-15
- Decaro N, Mari V, Campolo M, et al. Recombinant canine coronaviruses related to transmissible gastroenteritis virus of Swine are circulating in dogs. *J Virol.* 2009;83(3):1532-1537. doi:10.1128/JVI.01937-08
- Decaro N, Mari V, Elia G, Lanave G, Dowgier G, Colaianni ML, Martella V, Buonavoglia C. Full-length genome analysis of canine coronavirus type I. *Virus Res.* 2015;210:100-5. doi:10.1016/j.virusres.2015.07.018
- De Fine Licht HH. Does pathogen plasticity facilitate host shifts?. *PLoS Pathog.* 2018;14(5):e1006961. doi:10.1371/journal.ppat.1006961
- Drummond AJ, Ho SY, Phillips MJ, Rambaut A. Relaxed phylogenetics and dating with confidence. *PLoS Biol.* 2006;4(5):e88. doi:10.1371/journal.pbio.0040088
- Drummond AJ, Rambaut A, Shapiro B, Pybus OG. Bayesian coalescent inference of past population dynamics from molecular sequences. *Mol Biol Evol.* 2005;22(5):1185-1192. doi:10.1093/molbev/msi103
- Duchêne S, Duchêne D, Holmes EC, Ho SY. The Performance of the Date-Randomization Test in Phylogenetic Analyses of Time-Structured Virus Data. *Mol Biol Evol.* 2015;32(7):1895-1906. doi:10.1093/molbev/msv056
- Duckert P, Brunak S, Blom N. Prediction of proprotein convertase cleavage sites. *Protein Eng Des Sel.* 2004;17(1):107-112. doi:10.1093/protein/gzh013
- Forni D, Cagliani R, Clerici M, Sironi M. Molecular Evolution of Human Coronavirus Genomes. *Trends Microbiol.* 2017;25(1):35-48. doi:10.1016/j.tim.2016.09.001
- Herrewegh AA, Smeenk I, Horzinek MC, Rottier PJ, de Groot RJ. Feline coronavirus type II strains 79-1683 and 79-1146 originate from a double recombination between feline coronavirus type I and canine coronavirus. *J Virol.* 1998;72(5):4508-4514. doi:10.1128/JVI.72.5.4508-4514.1998
- Hou Y, Lin CM, Yokoyama M, Yount BL, Marthaler D, Douglas AL, Ghimire S, Qin Y, Baric RS, Saif LJ, Wang Q. Deletion of a 197-amino-acid region in the N-terminal domain of spike protein attenuates porcine epidemic diarrhea virus in piglets. *J Virol.* 2017;91(14):e002227-17. doi:10.1128/JVI.00227-17

Kalyaanamoorthy S, Minh BQ, Wong TKF, von Haeseler A, Jermiin LS. ModelFinder: fast model selection for accurate phylogenetic estimates. *Nat Methods*. 2017;14(6):587-589. doi:10.1038/nmeth.4285

Kass RE, & Adrian E. Raftery AE. Bayes Factors. *J. Am. Stat. Assoc.* 1995; 90(430), 773-795

Katoh K, Standley DM. MAFFT multiple sequence alignment software version 7: improvements in performance and usability. *Mol Biol Evol.* 2013;30(4):772-780. doi:10.1093/molbev/mst010

Kosakovsky Pond SL, Frost SD. Not so different after all: a comparison of methods for detecting amino acid sites under selection. *Mol Biol Evol.* 2005;22(5):1208-1222. doi:10.1093/molbev/msi105

Kosakovsky Pond SL, Poon AFY, Velazquez R, et al. HyPhy 2.5-A Customizable Platform for Evolutionary Hypothesis Testing Using Phylogenies. *Mol Biol Evol.* 2020;37(1):295-299. doi:10.1093/molbev/msz197

Kosakovsky Pond SL, Posada D, Gravenor MB, Woelk CH, Frost SD. GARD: a genetic algorithm for recombination detection. *Bioinformatics.* 2006;22(24):3096-3098. doi:10.1093/bioinformatics/btl474

Krempl C, Schultze B, Laude H, Herrler G. Point mutations in the S protein connect the sialic acid binding activity with the enteropathogenicity of transmissible gastroenteritis coronavirus. *J Virol.* 1997;71(4):3285-3287. doi:10.1128/JVI.71.4.3285-3287.1997

Kumar S, Stecher G, Li M, Knyaz C, Tamura K. MEGA X: Molecular Evolutionary Genetics Analysis across Computing Platforms. *Mol Biol Evol.* 2018;35(6):1547-1549. doi:10.1093/molbev/msy096

Lartillot N, Philippe H. Computing Bayes factors using thermodynamic integration. *Syst Biol.* 2006;55(2):195-207. doi:10.1080/10635150500433722

Li F. Structure, Function, and Evolution of Coronavirus Spike Proteins. *Annu Rev Virol.* 2016;3(1):237-261. doi:10.1146/annurev-virology-110615-042301

Liu C, Tang J, Ma Y, et al. Receptor usage and cell entry of porcine epidemic diarrhea coronavirus. *J Virol.* 2015;89(11):6121-6125. doi:10.1128/JVI.00430-15

Martin DP, Varsani A, Roumagnac P, et al. RDP5: a computer program for analyzing recombination in, and removing signals of recombination from, nucleotide sequence datasets. *Virus Evol.* 2020;7(1):veaa087. doi:10.1093/ve/veaa087.

McKeirnan AJ, Evermann JF, Hargis A, Ott RL. Isolation of feline coronaviruses from two cats with diverse disease manifestations. *Feline. Pract.* 1981;11:16-20.

Millet JK, Jaimes JA, Whittaker GR. Molecular diversity of coronavirus host cell entry receptors. *FEMS Microbiol Rev.* 2021;45(3):fuaa057. doi:10.1093/femsre/fuaa057

Minh BQ, Schmidt HA, Chernomor O, et al. IQ-TREE 2: New Models and Efficient Methods for Phylogenetic Inference in the Genomic Era [published correction appears in *Mol Biol Evol.* 2020 Aug 1;37(8):2461]. *Mol Biol Evol.* 2020;37(5):1530-1534. doi:10.1093/molbev/msaa015

Mozzi A, Biolatti M, Cagliani R, et al. Past and ongoing adaptation of human cytomegalovirus to its host. *PLoS Pathog.* 2020;16(5):e1008476. doi:10.1371/journal.ppat.1008476

Murrell B, Weaver S, Smith MD, et al. Gene-wide identification of episodic selection. *Mol Biol Evol.* 2015;32(5):1365-1371. doi:10.1093/molbev/msv035

Murrell B, Wertheim JO, Moola S, Weighill T, Scheffler K, Kosakovsky Pond SL. Detecting individual sites subject to episodic diversifying selection. *PLoS Genet.* 2012;8(7):e1002764. doi:10.1371/journal.pgen.1002764

Oka T, Saif LJ, Marthaler D, Esseili MA, Meulia T, Lin CM, Vlasova AN, Jung K, Zhang Y, Want Q. Cell culture isolation and sequence analyses of genetically diverse US porcine epidemic diarrhea virus strains including a novel strain with a large deletion in the spike gene. *Vet Microbiol.* 2014;173(3-4):258-269. doi:10.1016/j.vetmic.2014.08.012

Paaby AB, Rockman MV. Cryptic genetic variation: evolution's hidden substrate. *Nat Rev Genet.* 2014;15(4):247-258. doi:10.1038/nrg3688

Padidam M, Sawyer S, Fauquet CM. Possible emergence of new geminiviruses by frequent recombination. *Virology.* 1999;265(2):218-225. doi:10.1006/viro.1999.0056

Rambaut A, Drummond AJ, Xie D, Baele G, Suchard MA. Posterior Summarization in Bayesian Phylogenetics Using Tracer 1.7. *Syst Biol.* 2018;67(5):901-904. doi:10.1093/sysbio/syy032

Rambaut A, Lam TT, Max Carvalho L, Pybus OG. Exploring the temporal structure of heterochronous sequences using TempEst (formerly Path-O-Gen). *Virus Evol.* 2016;2(1):vew007. doi:10.1093/ve/vew007

Rasschaert D, Duarte M, Laude H. Porcine respiratory coronavirus differs from transmissible gastroenteritis virus by a few genomic deletions. *J Gen Virol.* 1990;71 (Pt 11):2599-2607. doi:10.1099/0022-1317-71-11-2599

Reguera J, Santiago C, Mudgal G, Ordoño D, Enjuanes L, Casasnovas JM. Structural bases of coronavirus attachment to host aminopeptidase N and its inhibition by neutralizing antibodies. *PLoS Pathog.* 2012;8(8):e1002859. doi:10.1371/journal.ppat.1002859

Rieux A, Khatchikian CE. tipdatingbeast: an R package to assist the implementation of phylogenetic tip-dating tests using beast. *Mol Ecol Resour.* 2017;17(4):608-613. doi:10.1111/1755-0998.12603

Sanchez CM, Pascual-Iglesias A, Sola I, Zuñiga S, Enjuanes L. Minimum Determinants of Transmissible Gastroenteritis Virus Enteric Tropism Are Located in the N-Terminus of Spike Protein. *Pathogens.* 2019;9(1):2. doi:10.3390/pathogens9010002

Sauer MM, Tortorici MA, Park YJ, et al. Structural basis for broad coronavirus neutralization. Preprint. *bioRxiv.* 2020;2020.12.29.424482. doi:10.1101/2020.12.29.424482

Schultze B, Krempf C, Ballesteros ML, et al. Transmissible gastroenteritis coronavirus, but not the related porcine respiratory coronavirus, has a sialic acid (N-glycolylneuraminic acid) binding activity. *J Virol.* 1996;70(8):5634-5637. doi:10.1128/JVI.70.8.5634-5637.1996

Sharif S, Arshad SS, Hair-Bejo M, Omar AR, Zeenathul NA, Hafidz MA. Prevalence of feline coronavirus in two cat populations in Malaysia. *J Feline Med Surg*. 2009;11(12):1031-1034. doi:10.1016/j.jfms.2009.08.005

Smith JM. Analyzing the mosaic structure of genes. *J Mol Evol*. 1992;34(2):126-129. doi:10.1007/BF00182389

Smith MD, Wertheim JO, Weaver S, Murrell B, Scheffler K, Kosakovsky Pond SL. Less is more: an adaptive branch-site random effects model for efficient detection of episodic diversifying selection. *Mol Biol Evol*. 2015;32(5):1342-1353. doi:10.1093/molbev/msv022

Stamatakis A. RAxML version 8: a tool for phylogenetic analysis and post-analysis of large phylogenies. *Bioinformatics*. 2014;30(9):1312-1313. doi:10.1093/bioinformatics/btu033

Sun XL. The Role of Cell Surface Sialic Acids for SARS-CoV-2 Infection [published online ahead of print, 2021 Apr 28]. *Glycobiology*. 2021;cwab032. doi:10.1093/glycob/cwab032

Tresnan DB, Levis R, Holmes KV. Feline aminopeptidase N serves as a receptor for feline, canine, porcine, and human coronaviruses in serogroup I. *J Virol*. 1996;70(12):8669-8674. doi:10.1128/JVI.70.12.8669-8674.1996

Vlasova AN, Diaz A, Dantie D, et al. Novel Canine Coronavirus Isolated from a Hospitalized Pneumonia Patient, East Malaysia [published online ahead of print, 2021 May 20]. *Clin Infect Dis*. 2021;ciab456. doi:10.1093/cid/ciab456

Wang C, van Haperen R, Gutiérrez-Álvarez J, et al. A conserved immunogenic and vulnerable site on the coronavirus spike protein delineated by cross-reactive monoclonal antibodies. *Nat Commun*. 2021;12(1):1715. doi:10.1038/s41467-021-21968-w

Wang S, Qiu Z, Hou Y, et al. AXL is a candidate receptor for SARS-CoV-2 that promotes infection of pulmonary and bronchial epithelial cells. *Cell Res*. 2021;31(2):126-140. doi:10.1038/s41422-020-00460-y

Wertheim JO, Murrell B, Smith MD, Kosakovsky Pond SL, Scheffler K. RELAX: detecting relaxed selection in a phylogenetic framework. *Mol Biol Evol*. 2015;32(3):820-832. doi:10.1093/molbev/msu400

Wesley RD. The S gene of canine coronavirus, strain UCD-1, is more closely related to the S gene of transmissible gastroenteritis virus than to that of feline infectious peritonitis virus. *Virus Res*. 1999;61(2):145-152. doi:10.1016/s0168-1702(99)00032-5

Whittaker GR, André NM, Millet JK. Improving Virus Taxonomy by Recontextualizing Sequence-Based Classification with Biologically Relevant Data: the Case of the *Alphacoronavirus* 1Species. *mSphere*. 2018;3(1):e00463-17. doi:10.1128/mSphereDirect.00463-17

Wong AHM, Tomlinson ACA, Zhou D, et al. Receptor-binding loops in alphacoronavirus adaptation and evolution. *Nat Commun*. 2017;8(1):1735. doi:10.1038/s41467-017-01706-x

Wu K, Li W, Peng G, Li F. Crystal structure of NL63 respiratory coronavirus receptor-binding domain complexed with its human receptor. *Proc Natl Acad Sci U S A*. 2009;106(47):19970-19974. doi:10.1073/pnas.0908837106

Yang TJ, Chang YC, Ko TP, et al. Cryo-EM analysis of a feline coronavirus spike protein reveals a unique structure and camouflaging glycans. *Proc Natl Acad Sci U S A*. 2020;117(3):1438-1446. doi:10.1073/pnas.1908898117

Yolitz J, Schwing C, Chang J, et al. Signal peptide of HIV envelope protein impacts glycosylation and antigenicity of gp120. *Proc Natl Acad Sci U S A*. 2018;115(10):2443-2448. doi:10.1073/pnas.1722627115